

# Is the annual maximum leaf area index an important driver of water fluxes simulated by a land surface model in temperate forests?

Audrey Maheu, Cybèle Cholet, Rebeca Cordero Montoya, and Louis Duchesne

**Abstract:** In land surface models, vegetation is often described using plant functional types (PFTs), a classification that aggregates plant species into a few groups based on similar characteristics. Within-PFT variability of these characteristics can introduce considerable uncertainty in the simulation of water fluxes in forests. Our objectives were to (i) compare the variability of the annual maximum leaf area index ( $LAI_{max}$ ) within and between PFTs and (ii) assess whether this variability leads to significant differences in simulated water fluxes at a regional scale. We classified our study region in southwestern Quebec (Canada) into three PFTs (evergreen needleleaf, deciduous broadleaf, and mixed forests) and characterized  $LAI_{max}$  using remotely sensed MODIS-LAI data. We simulated water fluxes with the Canadian Land Surface Scheme (CLASS) and performed a sensitivity analysis. We found that within-PFT variability of  $LAI_{max}$  was 1.7 times more important than variability between PFTs, with similar mean values for the two dominant PFTs, deciduous broadleaf forests ( $6.6 \text{ m}^2 \cdot \text{m}^{-2}$ ) and mixed forests ( $6.3 \text{ m}^2 \cdot \text{m}^{-2}$ ). In CLASS, varying  $LAI_{max}$  within the observed range of values ( $4.0\text{--}7.5 \text{ m}^2 \cdot \text{m}^{-2}$ ) led to changes of less than 2% in mean evapotranspiration. Overall,  $LAI_{max}$  is likely not an important driver of the spatial variability of water fluxes at the regional level.

**Key words:** leaf area index, plant functional type, land surface model, hydrology, temperate forest.

**Résumé :** Dans les modèles de surface terrestre, la végétation est souvent décrite en utilisant des types fonctionnels de plantes (TFP) qui regroupent les espèces de plantes dans quelques groupes sur la base de caractéristiques similaires. La variabilité de ces caractéristiques TFP peut introduire une incertitude considérable dans la simulation des flux hydriques en forêt. Nos objectifs consistaient à (i) comparer la variation de l'indice de surface foliaire annuel maximum ( $LAI_{max}$ ) au sein de et entre les TFP et (ii) déterminer si cette variabilité entraîne des différences significatives dans les flux hydriques simulés à une échelle régionale. La région à l'étude, située dans le sud-ouest du Québec (Canada), a été répartie selon trois TFP (forêt de conifères, forêt feuillue et forêt mixte) et nous avons caractérisé  $LAI_{max}$  à l'aide de données de télédétection MODIS-LAI. Nous avons simulé les flux hydriques avec le modèle CLASS et effectué une analyse de sensibilité. Nous avons trouvé que la variabilité de  $LAI_{max}$  au sein des TFP était 1,7 fois plus importante qu'entre les TFP. Les deux TFP dominants avaient des valeurs moyennes similaires :  $6,6 \text{ m}^2 \cdot \text{m}^{-2}$  dans les forêts feuillues et  $6,3 \text{ m}^2 \cdot \text{m}^{-2}$  dans les forêts mixtes. Dans le modèle CLASS, faire varier  $LAI_{max}$  au-delà de l'étendue des valeurs observées ( $4,0\text{--}7,5 \text{ m}^2 \cdot \text{m}^{-2}$ ) entraînait des changements inférieurs à 2 % dans l'évapotranspiration moyenne. Globalement,  $LAI_{max}$  n'était vraisemblablement pas un facteur important quant à la variabilité spatiale des flux hydriques à l'échelle régionale. [Traduit par la Rédaction]

**Mots-clés :** indice de surface foliaire, type fonctionnel de plantes, modèle de surface terrestre, hydrologie, forêt tempérée.

## 1. Introduction

Land surface models describe interactions between the atmosphere, land, and biosphere to simulate surface energy and water fluxes (Flato 2011). They are used to represent the lower boundary conditions of global or regional climate models (coupled or off-line) and thus are key to assessing the impacts of global change on forests. For example, land surface models have been used to investigate the impact of droughts (De Kauwe et al. 2015), fires (Lasslop et al. 2016), and pest invasions (Mikkelsen et al. 2013) on the energy and water budgets of forests.

In land surface models, vegetation is often described using a set of plant functional types (PFT). For global modelling purposes, plant species have been aggregated into a few PFTs based on

similar characteristics (e.g., growth and leaf forms, photosynthetic pathway) of ecosystem function (Wullschleger et al. 2014). An underlying principle of PFT is that form follows function (Box 1996), and for each PFT, fixed parameters are prescribed to describe both structural (e.g., minimum and maximum leaf area index, canopy height, maximum rooting depth) and physiological (e.g., minimum stomatal resistance) characteristics of vegetation.

This simplified representation of vegetation with PFTs was required to run global-scale simulations at a relatively coarse scale (~20–200 km). However, an enhancement in computational power has led to efforts to better capture the variability of energy and water fluxes (Fan et al. 2019). PFTs have been shown to broadly capture ecosystem function at the regional level (Chapin

Received 18 March 2020. Accepted 14 September 2020.

A. Maheu, C. Cholet, and R. Cordero Montoya. Institut des Sciences de la Forêt tempérée, Université du Québec en Outaouais, Ripon, QC J0V 1V0, Canada.  
L. Duchesne. Direction de la recherche forestière, Ministère des Forêts, de la Faune et des Parcs du Québec, Québec, QC G1P 3W8, Canada.

**Corresponding author:** Audrey Maheu (email: [audrey.maheu@uqo.ca](mailto:audrey.maheu@uqo.ca)).

Copyright remains with the author(s) or their institution(s). Permission for reuse (free in most cases) can be obtained from [copyright.com](http://copyright.com).

et al. 1996; Diaz and Cabido 1997; Kuiper et al. 2014). Nevertheless, various studies have assessed the variability of physiological characteristics within PFTs and found that the use of a PFT classification introduces considerable uncertainty in the simulation of carbon and water fluxes (Groenendijk et al. 2011). Indeed, trait variation of species within the same PFT can be larger than trait variation between different PFTs when describing plant photosynthesis and hydraulics (Anderegg 2015; Butler et al. 2017). While progress is being made on the handling of within-PFT variability of physiological characteristics (van Bodegom et al. 2014; Pappas et al. 2016; Matheny et al. 2017), the variability of structural characteristics within PFT has been little studied even though recent work has stressed the importance of structural diversity in explaining ecosystem function (LaRue et al. 2019).

Structural characteristics hold great importance in simulating energy and water fluxes in land surface models. For example, in the Canadian Land Surface Scheme (CLASS), leaf area index (LAI) is used to capture phenology and set to vary annually between minimum and maximum values prescribed for each PFT (Verseghy 2012). Canopy transmittance of solar radiation is assessed based on the plant area index (PAI, which considers the area of woody parts in addition to leaf area) and thus influences the simulation of snowmelt. LAI and PAI are also used as scaling factors when simulating transpiration and interception of precipitation, respectively. Given its central role in land surface models, LAI values assigned to PFTs can have a large impact on the simulation of water fluxes. For example, Oleson and Bonan (2000) have shown a mismatch between PFT-prescribed and remotely sensed LAI values in boreal forests and that the NCAR (National Center for Atmospheric Research) land surface model better captured the spatial variability of evapotranspiration when using remotely sensed data as an input. However, the sensitivity of evapotranspiration to LAI varies greatly between land surface models. Zhang et al. (2013) showed strong sensitivity of the CABLE-simulated evapotranspiration to  $\pm 50\%$  variations of LAI, particularly in North American broadleaf forests. On the other hand, Sullivan et al. (2019) computed evapotranspiration with remotely sensed data as input to a three-source Penman–Monteith model and found that evapotranspiration across the United States (including temperate forests) to be little sensitive to LAI, with a median change of +0.2% in evapotranspiration per percent change in LAI. These contrasting findings stress the need to better understand the influence of LAI on the spatial variability of water fluxes and stores in temperate forests, including at smaller regional scales.

We hypothesized that structural characteristics such as LAI are important drivers of the spatial variability of water fluxes in temperate forests, which a description of vegetation based on PFT fails to capture. Accordingly, we predicted that (i) the variability of the annual maximum LAI ( $LAI_{max}$ ) is larger within a given PFT than between PFTs and (ii) it will lead to significant differences in evapotranspiration and soil water content at the regional scale. To test these predictions, we characterized  $LAI_{max}$  using remote sensing data and then assessed the variability within and between PFTs (evergreen needleleaf, deciduous broadleaf, and mixed forests). We then investigated how observed variations of MODIS-derived  $LAI_{max}$  affected water fluxes and stores by performing a sensitivity analysis of a land surface model (CLASS).

## 2. Study area

We assessed the variability of  $LAI_{max}$  over the Outaouais administrative region (34 012 km<sup>2</sup>) in the southwestern portion of Quebec, Canada. The climate is classified as Dfb (snow, fully humid, warm summer) according to the Köppen–Geiger classification (Kottek et al. 2006). Mean annual temperatures (1981–2010) vary between 6.3 °C in the south and 1.7 °C in the north, while mean annual total precipitation varies from 900 mm in the west to 1100 mm in the east (McKenney et al. 2011). The Outaouais

region spans five bioclimatic domains, a classification performed by the Ministère des Forêts, de la Faune et des Parcs (MFFP) du Québec according to late-successional species in mesic sites. The southern portion of the region is characterized by deciduous broadleaf forests, and bioclimatic domains are dominated by sugar maple (*Acer saccharum*), with bitternut hickory (*Carya cordiformis*; 6% of the region area), basswood (*Tilia americana*; 16%), or yellow birch (*Betula alleghaniensis*, 42%) as companion species. The northern portion of the region is characterized by mixed forests, and bioclimatic domains are dominated by balsam fir (*Abies balsamea*) with yellow birch (34% of the region area) or white birch (*Betula papyrifera*; 2%) as companion species.

Using CLASS, we simulated the water balance of a site located in the Duchesnay forest (46°57'33"N, 71°40'25"W). Although this site falls outside the study area, we selected it because (i) long-term (2012–2018) hourly soil moisture data were available and (ii) climatic, vegetation, and soil characteristics are comparable to those observed in the Outaouais region. The climate at Duchesnay is also defined as Dfb, but is slightly cooler (mean annual air temperature = 2.5 °C) and wetter (mean annual total precipitation = 1300 mm) than in the study region. The vegetation corresponds to an uneven-aged deciduous forest dominated by sugar maple, American beech, and yellow birch (basal area of 21.2, 7.4, and 6.3 m<sup>2</sup>·ha<sup>-1</sup>, respectively, for diameter at breast height > 9.0 cm) growing on a ferro-humic podzol with a sandy loamy texture. At two sites (east and west, 100 m apart), soil water content was measured hourly using time-domain reflectometry (CS615, Campbell Scientific) with sensor rods inserted horizontally at four soil horizons (A: 6 and 7 cm deep; B: 30 and 34 cm deep; BC: 55 and 60 cm deep; C: 90 cm deep).

## 3. Materials and methods

### 3.1. Characterizing the annual maximum LAI

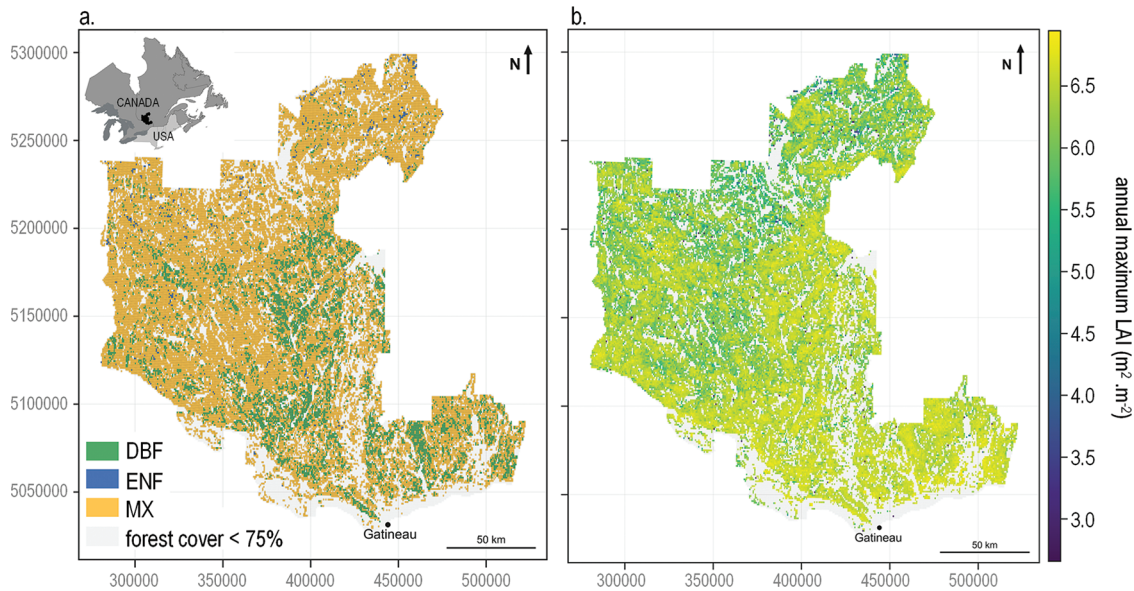
We characterized the LAI over the study area using the 8-day composite MODIS-LAI data with a 500 m resolution (Myneni et al. 2015) for the years 2002–2018. In this remote sensing dataset, the LAI is obtained by solving the three-dimensional radiative transfer equation using MODIS-retrieved data on reflectance in the red and near-infrared spectral bands as well as a global biome map. The MODIS-LAI dataset provides an estimate of the true LAI, equivalent to the LAI measured with direct methods (Yan et al. 2016).

Across the study area ( $n = 55\,327$  pixels), we selected forest-dominated areas — that is, grid cells with at least 75% of forest cover — which we assessed using the forest map of the fifth provincial forest inventory (MFFP 2018) regridded to a 500 m resolution. Accordingly, a total of 40 429 pixels were selected as forested area covering 24 380 km<sup>2</sup> of our study area. For each forested grid cell, we found the maximum LAI value for each year and then computed the mean  $LAI_{max}$ . Using satellite and flux tower observations as well as simulations from land surface models, various studies have investigated the temporal variability of LAI and how phenology influences surface fluxes in temperate forests (Anav et al. 2013; MacBean et al. 2015; Asaadi et al. 2018). In the present study, we were interested in the spatial variability of LAI and thus focused our analysis on a single metric,  $LAI_{max}$ .  $LAI_{max}$  holds great importance because it represents vegetation conditions that hold through much of the growing season, typically from late June to early September in deciduous broadleaf forests in eastern North America (Asaadi et al. 2018). Accordingly,  $LAI_{max}$  is associated with maximum evapotranspiration in these forests (Asaadi et al. 2018).

### 3.2. Assessing the regional-scale variability of the annual maximum LAI

In land surface models, PFTs are generally prescribed using a land cover map derived from remote sensing data (Sterling and

**Fig. 1.** (a) Plant functional type (DBF, deciduous broadleaf forest; ENF, evergreen needleleaf forest; MX, mixed forest) and (b) annual maximum LAI across the study area. The map was created with GeoPandas Python Package (Jordahl et al. 2019), and coordinates are UTM zone 18N. The inset was created with QGIS version 3.14 using a base map from the North American Atlas of Natural Resources Canada and the Base de données géographiques et administratives of the Ministère de l'Énergie et des Ressources naturelles. [Colour online.]



Ducharme 2008). Given the regional scale of our study, we defined PFTs based on the forest cover as defined by the provincial forest inventory: evergreen needleleaf forest (ENF), deciduous broadleaf forest (DBF), and mixed forest (MX; Fig. 1). Forest cover is defined according to the proportion of the basal area made up of needleleaf trees: ENF corresponds to forests where needleleaf trees make up more than 75% of the basal area, MX corresponds to forests where needleleaf trees make up between 25% and 74% of the basal area, and DBF correspond to forests where needleleaf trees make up less than 25% of the basal area (MFFP 2018). We characterized within- and between-PFT variability of  $LAI_{max}$  by comparing frequency distributions of ENF, DBF, and MX forests. We also computed the Fisher ratio, which is the ratio of between-class variability to within-class variability (Bishop 2006), as follows:

$$(1) \quad F = \frac{(\mu_1 - \mu_2)^2}{\sigma_1^2 + \sigma_2^2}$$

where  $\mu$  represents the mean,  $\sigma$  represents the standard deviation, and subscripts represent a given class. While an assessment of intraclass versus interclass variability typically relies on an analysis of variance (ANOVA), we did not perform such an analysis given our large sample size. Indeed, a large sample size often leads to small differences between classes being flagged as statistically significant. Instead, we assessed biological significance by performing a sensitivity analysis to assess how the observed range of variability of MODIS-derived  $LAI_{max}$  affected the simulation of soil moisture and evapotranspiration.

### 3.3. Description of the CLASS model

CLASS is a physically based land surface model (Verseghy 1991, 2012) that simulates heat and moisture exchanges between the surface and the atmosphere. It was initially developed to be run coupled to global or regional climate models, but offline simulations using forcing data from a standalone atmospheric model or from field measurements, as performed in this study, are also possible. In terms of forcing data, CLASS requires seven input variables at a 30 min time step: downwelling shortwave radiation,

downwelling longwave radiation, surface air pressure, air temperature, specific humidity, wind speed, and total precipitation. For each grid cell, CLASS computes the energy and water budgets separately over four subareas (bare soil, vegetation over bare soil, snowpack over bare soil, or vegetation over snowpack) and then averages it. For subareas with vegetation, CLASS considers the fractional coverage of four PFTs (needleleaf trees, broadleaf trees, crops, and grass). Physiological and structural characteristics are assigned representative values for each PFT, and these remain constant over the year except for the plant area index (PAI), which varies seasonally between set minimum and maximum values. Annual minimum and maximum PAI values are assigned to each PFT, and the LAI is then derived from these values: for crops and grass,  $LAI = PAI$ ; for needleleaf trees,  $LAI = 0.9 \times PAI$ ; and for broadleaf trees,  $LAI = PAI - \text{annual minimum PAI}$ . In CLASS, transpiration is a function of the LAI, while rain or snow interception as well as radiative transfer are a function of the PAI. Several soil layers can be defined in CLASS, each with specific thickness, texture, and organic matter content.

### 3.4. Water balance simulation at the Duchesnay forest

We used version 3.6 of CLASS within the hydrological land surface modelling platform Modélisation environnementale communautaire - Surface Hydrology (MESH; Pietroniro et al. 2007) developed by Environment and Climate Change Canada to simulate the soil water content and the evapotranspiration in the Duchesnay forest. Given the large gaps in observations from the local weather station, we used ERA5 reanalysis data (fifth-generation atmospheric reanalysis of the global climate released by the European Center for Medium-Range Weather Forecasts) as forcing data (Copernicus Climate Change Service 2017). We compared reanalysis data from 1981 to 2020 with observations from weather stations ( $n = 100$  for temperature,  $n = 113$  for precipitation) for an area that includes the Duchesnay forest and the Outaouais region (longitude: 79.5°W to 69.0°W; latitude: 44.0°N to 49.8°N) and found only small differences, with a mean absolute error of 8 mm for monthly total precipitation and 0.5 °C for monthly mean air temperature. Because the Duchesnay forest is composed primarily of broadleaf deciduous trees, the PFT

**Table 1.** Vegetation characteristics assigned to the deciduous broadleaf forest plant functional type at the Duchesnay study site.

	Deciduous broadleaf forest
PAI minimum ( $\text{m}^2 \cdot \text{m}^{-2}$ )	0.5
PAI maximum ( $\text{m}^2 \cdot \text{m}^{-2}$ )	6.0
Visible albedo	0.05
Near-infrared albedo	0.29
Minimum stomatal resistance ( $\text{s} \cdot \text{m}^{-1}$ )	125

was set to DBF. We set vegetation characteristics (Table 1) based on generic values for broadleaf cold deciduous forest provided in the CLASS documentation (Verseghy 2012), except for the rooting depth and roughness length. Rooting depth was set to 50 cm based on field observations. Roughness length was set to 2.1 m (recommended value is 2 m), corresponding to the forest canopy height extracted from the forest map of the fifth provincial forest inventory (MFFP 2018) divided by 10. The total soil depth was set to 1 m based on field observations; we discretized this soil column into five layers at depths of 0.1, 0.25, 0.45, 0.7, and 1.0 m. In CLASS, we defined the first soil layer (0–0.1 m) as organic, while the remaining soil layers were defined as mineral. We defined sand and clay content of each layer by averaging measurements from six profiles taken around the measurement sites.

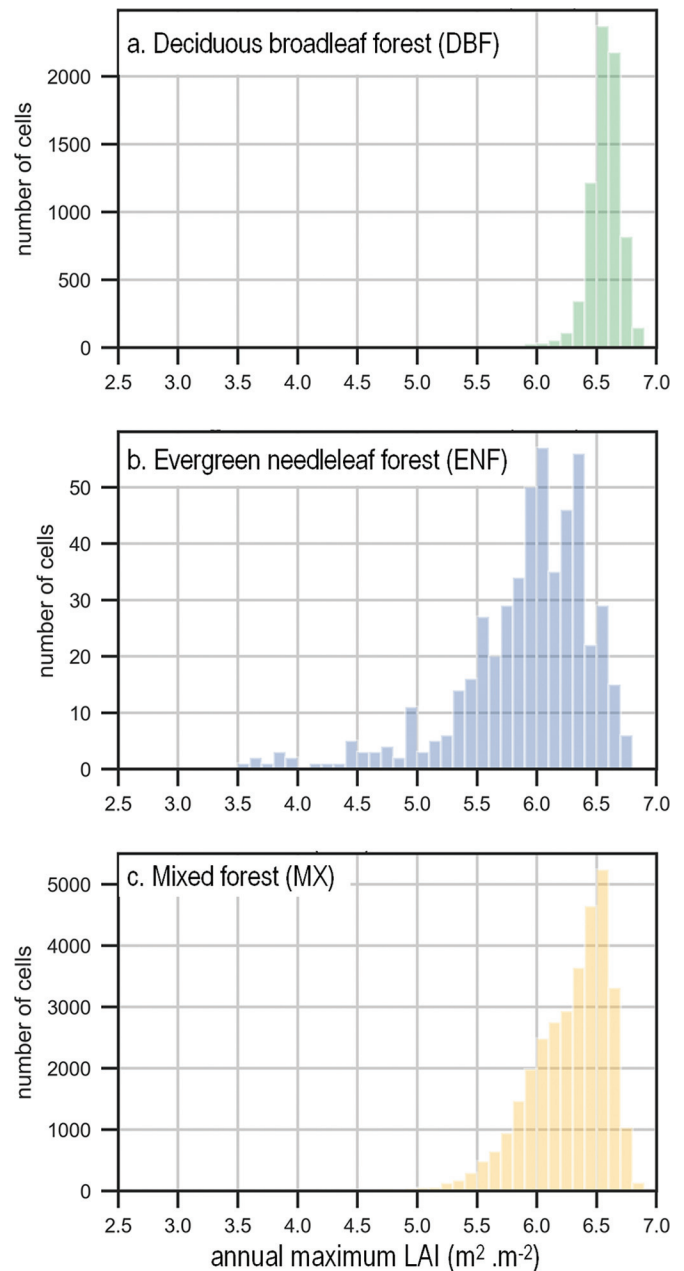
We assessed the performance of the model by comparing soil water content simulations to observations at three selected soil horizons. We compared the first two simulated soil layers (0–0.1 m and 0.1–0.25 m) to soil moisture measurements performed in the A and B horizons of the western site. Owing to discrepancies in observations at deeper horizons, we compared the third soil layer (0.25–0.45 m) to the BC horizon of the eastern site. We assessed the performance of the model by focusing on the snow-free period from May to October (MJJASO). We computed four performance metrics on a monthly basis to evaluate the ability of CLASS to simulate soil water content: root mean square error (RMSE), probability of detection index (POD), percent bias (Pbias), and Nash–Sutcliffe coefficient (NSE). The RMSE computes the mean difference between observed and simulated values; the closer its value is to zero, the better is the simulation. We used the POD to assess the ability of the model to simulate small values (defined as values below the 5th percentile) of soil water content:

$$(2) \quad \text{POD} = \frac{a}{a + b}$$

where  $a$  is the number of times that observed and simulated soil water contents are both below their respective 5th percentile and  $b$  is the number of times that observed soil water content is below its 5th percentile but simulated soil water content is not. The POD varies between zero and one; the closer its value is to one, the better is the simulation of small values. The Pbias assesses the mean tendency of simulated values to be larger (positive bias) or smaller (negative bias) than observations. NSE ranges between  $-\infty$  and 1, with NSE = 1 for a perfect fit between the model and observations, while negative values indicate that the mean value of observations offers a better predictor than the model.

Once the performance of the model had been validated, we performed a sensitivity analysis of the CLASS model. We simulated water fluxes and stores at Duchesnay forest by varying the annual maximum PAI ( $\text{PAI}_{\text{max}}$ ) between 4.0 and 7.5  $\text{m}^2 \cdot \text{m}^{-2}$  with increments of 0.5  $\text{m}^2 \cdot \text{m}^{-2}$ . When the canopy is fully developed, the LAI is comparable to the PAI in deciduous forests, with a difference of less than 0.75  $\text{m}^2 \cdot \text{m}^{-2}$  (Dufrière and Bréda 1995; Liu et al. 2015). A global analysis of broadleaf forests also found that the true LAI measured with direct methods was comparable to the effective

**Fig. 2.** Frequency distribution of the annual maximum leaf area index ( $\text{LAI}_{\text{max}}$ ) computed with 8-day composite MODIS-LAI data for the (a) deciduous broadleaf forest (DBF), (b) evergreen needleleaf forest (ENF), and (c) mixed forest (MX) in the study area. [Colour online.]



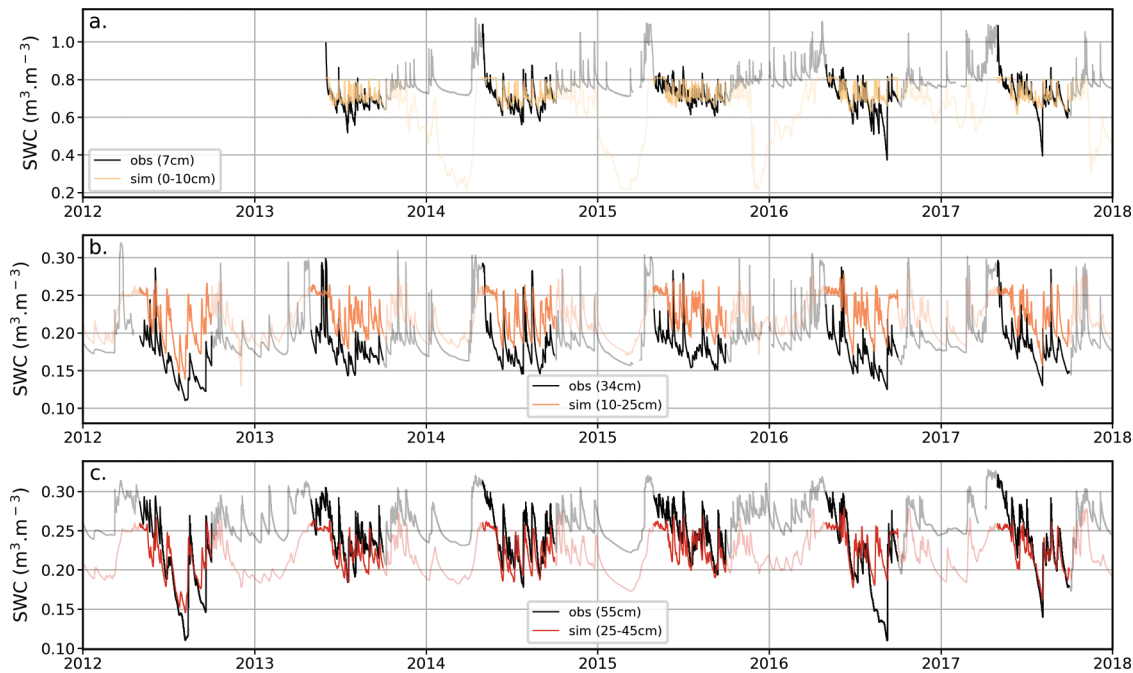
LAI that considers light interception by woody parts and assumes a random foliage distribution (bias <10%; Fang et al. 2012). Giving these findings, a sensitivity analysis of CLASS based on variations of  $\text{PAI}_{\text{max}}$  can appropriately reflect variations of  $\text{LAI}_{\text{max}}$ .

## 4. Results and discussion

### 4.1. Regional scale variability of the annual maximum LAI

Across the study region, MX was the dominant forest cover, representing 80.6% of the forest-dominated areas of the study region (Fig. 1a). DBF represented 18.1% of forest-dominated areas and was concentrated in the southeastern part of the study region. ENF was found in only a small portion of the study region

**Fig. 3.** Observations (obs) and simulations (sim) of soil water content (SWC) at the Duchesnay forest for three simulated soil layers: (a) 0–10 cm, (b) 10–25 cm, and (c) 25–45 cm. The focus of the study was on the period from May to October (MJJASO). Data are shown in light colours for the period from November to April. [Colour online.]



(1.3%), with most occurrences found in the northern area of the study region.  $LAI_{max}$  varied between 2.7 and 6.9  $m^2 \cdot m^{-2}$ , although when considering the 5th and 95th percentiles, most values fell between 5.7 and 6.7  $m^2 \cdot m^{-2}$ .  $LAI_{max}$  decreased with latitude, and we observed most values  $< 5.5 m^2 \cdot m^{-2}$  in the northern portion of the study region (Fig. 1b). Over a few grid cells ( $n = 113$ ),  $LAI_{max}$  was equal to zero over areas where forest cover exceeded 75% based on the provincial inventory data. This minor mismatch could be due to small differences in the delineation of waterbodies by the two datasets, and we removed these values when performing analyses.

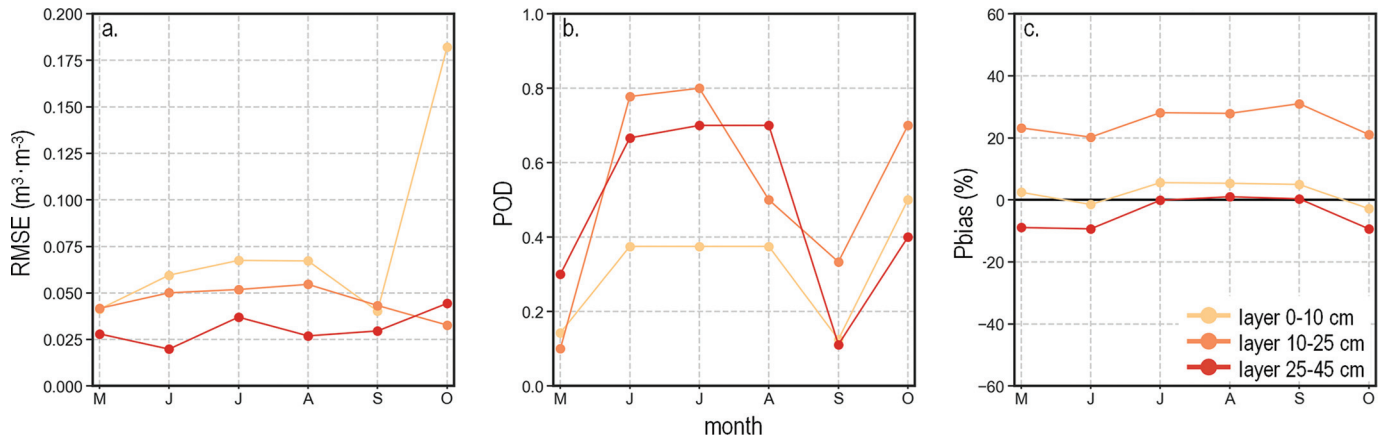
We observed little variability in  $LAI_{max}$  between the two dominant PFTs, as shown by the similar frequency histograms between DBF and MX (Fig. 2). Mean  $LAI_{max}$  was similar between DBF (6.6  $m^2 \cdot m^{-2}$ ) and MX (6.3  $m^2 \cdot m^{-2}$ ), although lower values were reached for MX (25th percentile = 6.1  $m^2 \cdot m^{-2}$ ) than for DBF (25th percentile = 6.5  $m^2 \cdot m^{-2}$ ). Mean  $LAI_{max}$  was slightly lower for ENF (5.9  $m^2 \cdot m^{-2}$ ) than for the two other PFTs. However, ENF represented forest cover of only 1.3% of the study region and is mainly associated with nonmesic conditions, thus offering a poor comparison to the two other PFTs. The mean  $LAI_{max}$  for the study region (6.3  $m^2 \cdot m^{-2}$ ) was comparable to the mean value compiled by Breuer et al. (2003) from LAI measurements in temperate deciduous forests in North America (6.5  $m^2 \cdot m^{-2}$ ), but larger than the mean  $LAI_{max}$  compiled by Iio et al. (2014) using a global dataset (4.9  $m^2 \cdot m^{-2}$ ). MODIS-derived values of  $LAI_{max}$  appeared slightly greater than values from global datasets of land surface parameters. For example, the  $LAI_{max}$  derived for the deciduous broadleaf forest PFT in the CLASS documentation, with annual maximum and minimum PAI values of 6.0 and 0.5  $m^2 \cdot m^{-2}$ , respectively, corresponds to a  $LAI_{max}$  of 5.5  $m^2 \cdot m^{-2}$ . Even lower values are observed from the global dataset compiled from Hagemann (2002), with the southern portion of the study region made up of cool broadleaf forest ( $LAI_{max} = 5.2 m^2 \cdot m^{-2}$ ) and the northern portion made up of cool mixed forest ( $LAI_{max} = 4.3 m^2 \cdot m^{-2}$ ).

Although within-PFT variability was relatively small for DBF (standard deviation = 0.14  $m^2 \cdot m^{-2}$ ), we observed larger within-PFT variability for MX (standard deviation = 0.34  $m^2 \cdot m^{-2}$ ) and ENF (standard deviation = 0.56  $m^2 \cdot m^{-2}$ ; Fig. 2). The Fisher ratio (eq. 1) between the two dominant PFTs (DBF and MX) was equal to 0.6, thus showing that within-PFT variability was 1.7 times larger than between-PFT variability. Within-PFT variability over the study region was smaller than that observed globally, with compilations of LAI measurements in deciduous forests reporting standard deviation close to 1.6  $m^2 \cdot m^{-2}$  (Breuer et al. 2003; Iio et al. 2014). The maximum LAI has been shown to vary with temperature and water availability on a global scale (Iio et al. 2014) and, as such, the smaller within-PFT variability can be traced back to the relatively small climate variability observed over the study region.

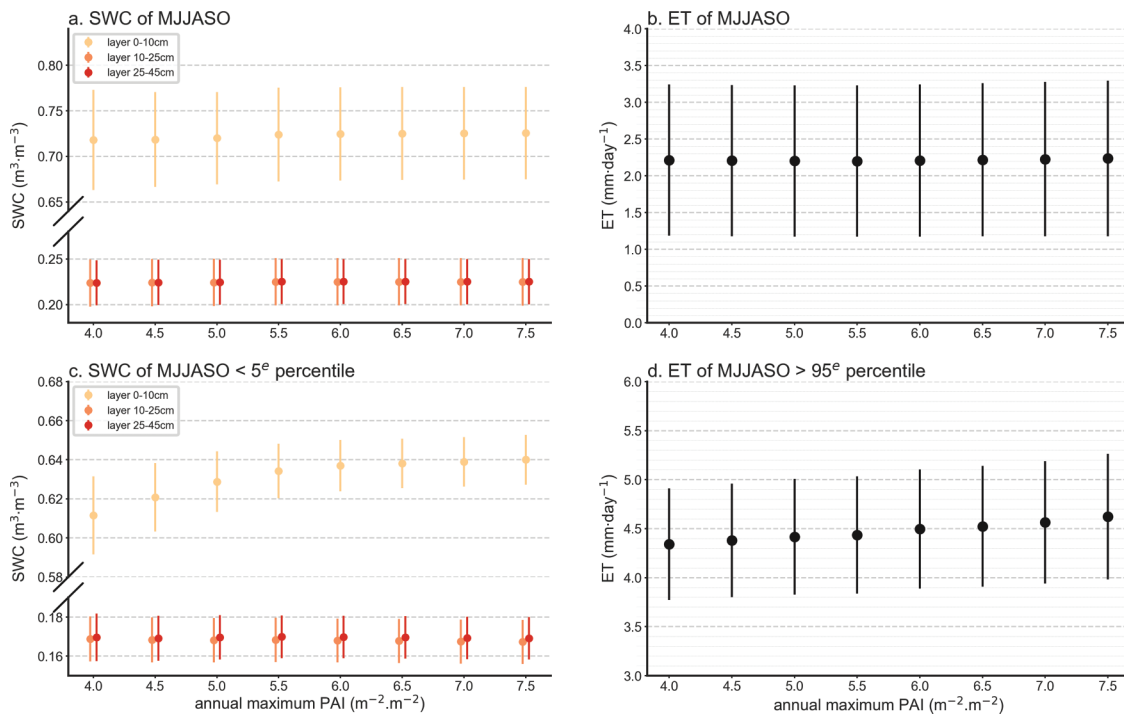
#### 4.2. Performance of the CLASS model

Figure 3 shows the simulation of soil moisture with CLASS, with a focus on the period from May to October, when variability in the  $LAI_{max}$  is likely to have the most influence on the water balance. Little consideration should be given to soil moisture outside of this period given the issues with time-domain reflectometry measurement of soil moisture at near-freezing temperatures (Kahimba and Ranjan 2007). Figure 4 shows the various metrics used to assess the performance of the model, with the exception of the NSE, which was often negative. The evaluation of soil moisture modelling is notably difficult, as soil properties and thus soil moisture can vary on a very small scale, both horizontally and vertically (Famiglietti et al. 2008; Vereecken et al. 2010; Gwak and Kim 2017). Varying soil properties can lead to a shift between observations and simulations, as is the case for the second soil layer, where the Pbias exceeded 20%. In the present study, model performance is also affected by the fact that we used reanalysis as opposed to local meteorological data to represent meteorological forcing. Indeed, we can sometimes observe a mismatch between observed and simulated soil moisture, as was the case in summer 2016, when the reanalysis data did not capture a

**Fig. 4.** Performance metrics (a) root mean square error (RMSE), (b) probability of detection (POD), and (c) percent bias (Pbias) comparing observations and simulations of soil water content at the Duchesnay forest at three simulated soil layers (0–10 cm, 10–25 cm, and 25–45 cm) for the period from May to November (MJJASO). [Colour online.]



**Fig. 5.** Mean and standard deviation of simulated water fluxes and stores for varying values of the annual maximum plant area index ( $\text{PAI}_{\text{max}}$ ) for the period from May to November (MJJASO). Panels represent simulated values of (a) soil water content (SWC), (b) evapotranspiration (ET), (c) 5th percentile of soil water content, and (d) 95th percentile of evapotranspiration. [Colour online.]



prolonged dry period. The model performed best at the deepest soil layer (Fig. 3c), and the NSE varied from 0.34 to 0.61 between June and August. As is the case for other soil layers, performance declined at the beginning (May) and end (September and October) of the study period. At the deepest soil layer, the model captured the large reduction in soil moisture below  $0.15 \text{ m}^3 \cdot \text{m}^{-3}$  during the summers of 2012 and 2017, although it failed to do so in 2016. Still, the POD index shows the ability of the model to simulate the soil moisture drawdown during the growing season. Indeed, the best performance (POD between 0.5 and 0.8 for layers 2 and 3) was found for the June to August period. It is particularly relevant for the present study given that we could expect soil moisture to be particularly sensitive to variations in  $\text{LAI}_{\text{max}}$  during this period.

### 4.3. Sensitivity analysis

Variation of  $\text{PAI}_{\text{max}}$  between 4.0 and 7.5  $\text{m}^2 \cdot \text{m}^{-2}$  had little impact on mean simulated values of water fluxes and stores between May and October at the Duchesnay site (Figs. 5a–5b). We observed variations of less than 2% between mean values of soil moisture as well as between mean values of evapotranspiration. For example, daily mean evapotranspiration remained close to 2.2 mm when varying the  $\text{PAI}_{\text{max}}$ .  $\text{LAI}_{\text{max}}$  is thus not likely to be an important driver of the spatial variability of simulated water fluxes and stores in the study area. Indeed, the model showed little sensitivity over the range of simulated  $\text{PAI}_{\text{max}}$  values (4.0–7.5  $\text{m}^2 \cdot \text{m}^{-2}$ ), which was larger than the variability of MODIS-derived  $\text{LAI}_{\text{max}}$  over the study region (5th and 95th percentiles = 5.7 and 6.7  $\text{m}^2 \cdot \text{m}^{-2}$ , respectively). These findings generally agree with

sensitivity analyses performed with land surface models at Ameriflux sites, where mean evapotranspiration in broadleaf forests was found to be relatively insensitive to site-level variations in LAI (Puma et al. 2013; Ukkola et al. 2016). Instead, LAI mainly influenced the model's partitioning of evapotranspiration into evaporation and transpiration rather than affecting the magnitude of the simulated flux (Puma et al. 2013). While the partitioning of evapotranspiration has indeed been linked to LAI (Wang et al. 2014; Wei et al. 2017), recent evidence suggests that the fraction of transpiration is independent of LAI when vegetation is in equilibrium with the local climate (Paschalis et al. 2018). Indeed, this could explain the low sensitivity of simulated water fluxes to LAI observed in the present study, given that the sensitivity analysis focused on dense forests near equilibrium conditions ( $4.0 \text{ m}^2 \cdot \text{m}^{-2} \leq \text{LAI}_{\text{max}} \leq 7.5 \text{ m}^2 \cdot \text{m}^{-2}$ ).

Because  $\text{LAI}_{\text{max}}$  rarely dropped below  $4 \text{ m}^2 \cdot \text{m}^{-2}$  in our study region, we did not investigate the sensitivity of water fluxes to smaller LAI values. In boreal forests, LAI has been found to be an important scaling parameter of eddy-covariance measurements of evapotranspiration, but only in sparse forest stands ( $\text{LAI} < 3 \text{ m}^2 \cdot \text{m}^{-2}$ ) (Launiainen et al. 2016). Similar to our findings, evapotranspiration in denser boreal forest stands was little influenced by LAI; instead, it was strongly coupled to species traits as well as to site and weather conditions. Empirical evidence from forest thinning experiments at the stand level (Bréda et al. 1995; Gebhardt et al. 2014) or vegetation removal in paired catchment experiments (Bosch and Hewlett 1982; Brown et al. 2005) indicate that a large reduction in LAI results in decreased evapotranspiration. However, very little empirical evidence exists on the sensitivity of evapotranspiration to LAI in dense forests. Such data would help situate the minimal response to changes in LAI for evapotranspiration simulated by CLASS (present study) as well as by other land surface models (Puma et al. 2013; Ukkola et al. 2016) in deciduous broadleaf forests. Indeed, validating simulations by land surface models with empirical data are particularly important given recently diagnosed deficiencies in the covariation of LAI and turbulent fluxes in five land surface models (Forzieri et al. 2018).

While we found mean values to be relatively insensitive to changes in  $\text{PAI}_{\text{max}}$ , extreme values of water fluxes and stores simulated by CLASS were slightly sensitive to vegetation structure. Under dry conditions (soil water content below the 5th percentile), the surface soil layer was the most sensitive to changes in  $\text{PAI}_{\text{max}}$ , with mean soil moisture varying between 0.61 and  $0.63 \text{ m}^3 \cdot \text{m}^{-3}$  between May and October, while we observed little variation for deeper soil layers (Fig. 5c). In the surface soil layer, minimum soil moisture concurred with the lower simulated value of  $\text{PAI}_{\text{max}}$  ( $4.0 \text{ m}^3 \cdot \text{m}^{-3}$ ). This pattern may appear counterintuitive, as one could expect lower soil moisture to concur with larger  $\text{PAI}_{\text{max}}$  values as a result of increased evapotranspiration. When considering days where daily evapotranspiration exceeded the 95th percentile, we did observe an increase in evapotranspiration with  $\text{PAI}_{\text{max}}$ : mean evapotranspiration increased from  $4.3 \text{ mm} \cdot \text{day}^{-1}$  for a  $\text{PAI}_{\text{max}}$  of  $4.0 \text{ m}^2 \cdot \text{m}^{-2}$  to  $4.7 \text{ mm} \cdot \text{day}^{-1}$  for a  $\text{PAI}_{\text{max}}$  of  $7.5 \text{ m}^2 \cdot \text{m}^{-2}$  (Fig. 5d). However, the observed increase in surface soil water content with increasing  $\text{PAI}_{\text{max}}$  values has previously been documented when simulating soil moisture with CLASS (Isabelle et al. 2018). This pattern can be traced back to an increase in evaporation at the soil surface under a sparser canopy. Similar to our findings, Puma et al. (2013) found that extremes of water fluxes were sensitive to changes ( $\pm 30\%$ ) in LAI in a broadleaf forest, even though mean evapotranspiration was relatively insensitive. Indeed, evapotranspiration in broadleaf forests has been found to be particularly sensitive to LAI during rainfall deficits (Ukkola et al. 2016). In the present study, the period considered included three particularly dry summers (2012, 2016, and 2017), which could explain why soil moisture simulations exhibited a certain sensitivity to  $\text{PAI}_{\text{max}}$  (Fig. 5c).

#### 4.4. Limitations

The objective of this study was to investigate spatial variability in LAI. To do so, we derived  $\text{LAI}_{\text{max}}$  using remote sensing data, as it allowed the retrieval of LAI over large areas. Remote sensing methods do not provide a direct measurement of LAI. Instead, reflectance values measured by optical sensors are converted into estimates of LAI using biome-specific empirical transfer functions (Fang et al. 2019). This method is imperfect owing to the uncertainty in reflectance values associated with atmospheric conditions as well as errors in land cover data used as ancillary information for biome classification. In woody biomes, the RMSE of MCD5 MODIS data amounted to  $1.05 \text{ m}^2 \cdot \text{m}^{-2}$  when compared against 57 field measurements across the globe (Fang et al. 2012). A similar value (RMSE =  $0.96 \text{ m}^2 \cdot \text{m}^{-2}$ ) was found for broadleaf forests but for a limited number of field measurements ( $n = 7$ ). Overall, the uncertainty of MODIS-derived  $\text{LAI}_{\text{max}}$  would likely have little impact on simulated water fluxes in dense forests given that CLASS showed minimal sensitivity (less than 2% changes in mean evapotranspiration; Fig. 5) when varying  $\text{LAI}_{\text{max}}$  between  $4.0$  and  $7.5 \text{ m}^2 \cdot \text{m}^{-2}$ . Instead, the mismatch in  $\text{LAI}_{\text{max}}$  between MODIS-derived values and global PFT datasets appears to be a greater source of uncertainty. Indeed, we found differences of up to  $2 \text{ m}^2 \cdot \text{m}^{-2}$  between MODIS-derived  $\text{LAI}_{\text{max}}$  and global PFT  $\text{LAI}_{\text{max}}$ , highlighting the need to define regionally specific PFT values in regional applications of land surface models.

Owing to constraints in data availability, the site of the water balance simulation (Duchesnay forest) was located outside of the study region (Outaouais region) where we investigated the spatial variability of  $\text{LAI}_{\text{max}}$ . The Outaouais region receives less precipitation (mean annual total precipitation between 900 and 1100 mm) than the Duchesnay forest (mean annual total precipitation = 1300 mm). Compared with the Duchesnay forest, the drier climate of the Outaouais region may lead to higher levels of competition for water resources and thus result in greater sensitivity of simulated water fluxes to forest density (i.e.,  $\text{LAI}_{\text{max}}$ ) in the CLASS model.

In the present study, we focused our analysis on a single metric,  $\text{LAI}_{\text{max}}$ , because our objective was to (i) investigate spatial variability (as opposed to temporal variability) in LAI and because (ii) the CLASS model requires only annual minimum and maximum LAI as input. As such,  $\text{LAI}_{\text{max}}$  was computed as a multi-year mean, and we did not consider interannual variability. Forzieri et al. (2017) explored interannual variations in LAI and energy fluxes (including the latent heat flux associated with evapotranspiration) and found that vegetation density had a substantial impact on surface fluxes at the global scale between 1982 and 2011. As such, further work is needed to quantify interannual variability of  $\text{LAI}_{\text{max}}$  at the regional scale and account for it in land surface models such as CLASS.

#### 4.5. Further work

The sensitivity analysis performed in the present study is specific to CLASS, although simulations with other land surface models came to similar conclusions regarding the relatively small influence of LAI on the simulation of water fluxes in dense deciduous broadleaf forests (Puma et al. 2013; Ukkola et al. 2016). The sensitivity of land surface models to LAI can be highly variable, as demonstrated by a comparison at the global level of 27 land surface models participating in CMIP5 (Zeng et al. 2016). Moreover, evidence from observations (Forzieri et al. 2018) and simulations (Lu et al. 2013) suggest that sensitivity to LAI not only varies between models but is also PFT dependent. For example, simulated annual evapotranspiration was most sensitive to LAI in evergreen and deciduous needleleaf forests, while LAI explained only 5% of the variance in simulated annual evapotranspiration in deciduous broadleaf forests (Lu et al. 2013). These findings stress the need to better understand within-PFT variability of LAI for

other PFTs, notably those associated with the largest sensitivity to changes in LAI.

A greening trend — that is, an increase of 8% in LAI at the global level — has been observed between the 1980s and the 2010s (Zeng et al. 2018). Based on climate model simulations, this greening trend has been associated with a 12 mm·year<sup>-1</sup> increase in both evapotranspiration and precipitation over the same period (Zeng et al. 2018). Overall, this greening trend shows the importance of further work to understand the interplay between LAI and water fluxes in order to predict the impacts of climate change on the water cycle. In temperate forests of eastern North America, the greening trend amounted to ~0.06 m<sup>2</sup>·m<sup>-2</sup>·year<sup>-1</sup> for the 1982–2009 period and appeared to be mainly driven by land cover changes and a CO<sub>2</sub> fertilization effect (Zhu et al. 2016). In these forests, considerable variability was found at the regional scale in terms of both the magnitude of the greening trend and its driving factors. Most studies on the Earth's greening trend have been performed at the global scale (Zhu et al. 2016; Forzieri et al. 2017; Zeng et al. 2018). Going forward, studies at the regional scale are needed to assess the potential impacts of this greening trend on water fluxes. Indeed, as the present study suggests, the observed greening trend may have minimal influence on water fluxes in dense deciduous broadleaf forests given the minimal sensitivity of simulated evapotranspiration to LAI.

## 5. Conclusion

This study showed that vegetation structure, as characterized by LAI<sub>max</sub>, is likely not an important driver of the spatial variability of water fluxes simulated by the CLASS land surface model in temperate forests. Our results showed that within-PFT variability of LAI<sub>max</sub> was more important than variability between the two dominant PFTs (DBF and MX). However, contrary to what we predicted, a sensitivity analysis performed with the CLASS land surface model showed that the variability in MODIS-derived LAI<sub>max</sub> at a regional scale (5th and 95th percentiles = 5.7 and 6.7 m<sup>2</sup>·m<sup>-2</sup>, respectively) would have little influence on simulated mean water fluxes (evapotranspiration) and stores (soil water content). Modest sensitivity was observed when simulating evapotranspiration only under dry conditions (soil water content below the 5th percentile) in sparse forests (LAI<sub>max</sub> < 5 m<sup>2</sup>·m<sup>-2</sup>).

Instead of PFTs, remotely sensed LAI data have been used as a direct input to land surface models, leading to improvements in the simulation of water fluxes (Buermann et al. 2001; Bonan et al. 2002; Kang et al. 2007). While this finding may hold in certain regions and for certain PFTs, our study suggests that the use of remote sensing data to describe LAI<sub>max</sub> would likely not improve our ability to capture the spatial variability of evapotranspiration at a 500 m scale. As such, the use of PFTs to describe vegetation structure, a computationally efficient approach to describing vegetation, appears largely sufficient for simulating water fluxes and stores at such a scale across the study region. Still, the use of globally defined PFTs can lead to an underestimation of LAI<sub>max</sub>, with differences close to 2 m<sup>2</sup>·m<sup>-2</sup> between MODIS-derived regional values and global datasets of land surface parameters. As the resolution of land surface models is increasing, and as these models are increasingly being used for regional applications, our results suggest the need to adapt the representation of vegetation with regionally specific values. As such, remotely sensed data offer a practical way to compile regionally relevant values that can then be assigned to PFTs.

## Acknowledgements

This research was supported by the Ministère des Forêts, de la Faune et des Parcs (MFFP) du Québec. We thank Daniel Princz (University of Saskatchewan) for help with the implementation of CLASS within MESH. We also thank J. Gagné, M. Saint-Germain,

J.-P. Mottard, and P. Desjardins for performing the field work to monitor the Duchesnay site.

## References

- Anav, A., Murray-Tortarolo, G., Friedlingstein, P., Sitch, S., Piao, S., and Zhu, Z. 2013. Evaluation of land surface models in reproducing satellite derived leaf area index over the high-latitude northern hemisphere. Part II: Earth system models. *Remote Sens.* 5: 3637–3661. doi:10.3390/rs5083637.
- Anderegg, W.R.L. 2015. Spatial and temporal variation in plant hydraulic traits and their relevance for climate change impacts on vegetation. *New Phytol.* 205(3): 1008–1014. doi:10.1111/nph.12907. PMID:25729797.
- Asaadi, A., Arora, V.K., Melton, J.R., and Bartlett, P. 2018. An improved parameterization of leaf area index (LAI) seasonality in the Canadian Land Surface Scheme (CLASS) and Canadian Terrestrial Ecosystem Model (CTEM) modelling framework. *Biogeosciences*, 15: 6885–6907. doi:10.5194/bg-15-6885-2018.
- Bishop, C.M. 2006. *Pattern recognition and machine learning*. Springer, Singapore.
- Bonan, G.B., Levis, S., Kergoat, L., and Oleson, K.W. 2002. Landscapes as patches of plant functional types: An integrating concept for climate and ecosystem models. *Global Biogeochem. Cycles*, 16(2): 5–1–5–23. doi:10.1029/2000GB001360.
- Bosch, J.M., and Hewlett, J.D. 1982. A review of catchment experiments to determine the effect of vegetation changes on water yield and evapotranspiration. *J. Hydrol.* 55(1–4): 3–23. doi:10.1016/0022-1694(82)90117-2.
- Box, E.O. 1996. Plant functional types and climate at the global scale. *J. Veg. Sci.* 7(3): 309–320. doi:10.2307/3236274.
- Bréda, N., Granier, A., and Aussenac, G. 1995. Effects of thinning on soil and tree water relations, transpiration and growth in an oak forest (*Quercus petraea* (Matt.) Liebl.). *Tree Physiol.* 15: 295–306. doi:10.1093/treephys/15.5.295. PMID:14965953.
- Breuer, L., Eckhardt, K., and Frede, H.-G. 2003. Plant parameter values for models in temperate climates. *Ecol. Modell.* 169(2–3): 237–293. doi:10.1016/S0304-3800(03)00274-6.
- Brown, A.E., Zhang, L., McMahon, T.A., Western, A.W., and Vertessy, R.A. 2005. A review of paired catchment studies for determining changes in water yield resulting from alterations in vegetation. *J. Hydrol.* 310(1–4): 28–61. doi:10.1016/j.jhydrol.2004.12.010.
- Buermann, W., Dong, J., Zeng, X., Myneni, R.B., and Dickinson, R.E. 2001. Evaluation of the utility of satellite-based vegetation leaf area index data for climate simulations. *J. Climate*, 14(17): 3536–3550. doi:10.1175/1520-0442(2001)014<3536:EOTUOS>2.0.CO;2.
- Butler, E.E., Datta, A., Flores-Moreno, H., Chen, M., Wythers, K.R., Fazayeli, F., et al. 2017. Mapping local and global variability in plant trait distributions. *Proc. Natl. Acad. Sci.* 114(51): E10937–E10946. doi:10.1073/pnas.1708984114. PMID:29196525.
- Chapin, F.S., III, Bret-Harte, M.S., Hobbie, S.E., and Zhong, H. 1996. Plant functional types as predictors of transient responses of arctic vegetation to global change. *J. Veg. Sci.* 7: 347–358. doi:10.2307/3236278.
- Copernicus Climate Change Service. 2017. ERA5: Fifth generation of ECMWF atmospheric reanalyses of the global climate. Copernicus Climate Change Service Climate Data Store (CDS). Available from <https://cds.climate.copernicus.eu/cdsapp#!/home>.
- De Kauwe, M.G., Zhou, S.X., Medlyn, B.E., Pitman, A.J., Wang, Y.P., Duursma, R.A., and Prentice, I.C. 2015. Do land surface models need to include differential plant species responses to drought? Examining model predictions across a mesic-xeric gradient in Europe. *Biogeosciences*, 12(24): 7503–7518. doi:10.5194/bg-12-7503-2015.
- Diaz, S., and Cabido, M. 1997. Plant functional types and ecosystem function in relation to global change. *J. Veg. Sci.* 8(4): 463–474. doi:10.2307/3237198.
- Dufréne, E., and Bréda, N. 1995. Estimation of deciduous forest leaf area index using direct and indirect methods. *Oecologia*, 104(2): 156–162. doi:10.1007/BF00328580.
- Famiglietti, J.S., Ryu, D., Berg, A.A., Rodell, M., and Jackson, T.J. 2008. Field observations of soil moisture variability across scales. *Water Resour. Res.* 44: W01423. doi:10.1029/2006WR005804.
- Fan, Y., Clark, M., Lawrence, D.M., Swenson, S., Band, L.E., Brantley, S.L., et al. 2019. Hillslope hydrology in global change research and earth system modeling. *Water Resour. Res.* 55(2): 1737–1772. doi:10.1029/2018WR023903.
- Fang, H., Wei, S., and Liang, S. 2012. Validation of MODIS and CYCLOPES LAI products using global field measurement data. *Remote Sens. Environ.* 119: 43–54. doi:10.1016/j.rse.2011.12.006.
- Fang, H., Bar, F., Plummer, S., and Schapman-Strub, G. 2019. An overview of global leaf area index (LAI): Methods, products, validation and applications. *Rev. Geophys.* 57: 739–799. doi:10.1029/2018RG000608.
- Flato, G.M. 2011. Earth system models: an overview. *Wiley Interdiscip. Rev. Clim. Change*, 2: 783–800. doi:10.1002/wcc.148.
- Forzieri, G., Alkama, R., Miralles, D.G., and Cescatti, A. 2017. Satellites reveal contrasting responses of regional climate to the widespread greening of Earth. *Science*, 356: 1180–1184. doi:10.1126/science.aal1727. PMID:28546316.
- Forzieri, G., Duveiller, G., Georgievski, G., Li, W., Robertson, E., Kautz, M., et al. 2018. Evaluating the interplay between biophysical processes and

- leaf area changes in land surface models. *J. Adv. Model. Earth Syst.* **10**: 1102–1126. doi:10.1002/2018MS001284. PMID:30034575.
- Gebhardt, T., Häberler, K.-H., Matussek, R., Schulz, C., and Ammer, C. 2014. The more, the better? Water relations of Norway spruce stands after progressive thinning. *Agric. For. Meteorol.* **197**: 235–243. doi:10.1016/j.agrformet.2014.05.013.
- Groenendijk, M., Dolman, A.J., van der Molen, M.K., Leuning, R., Arneth, A., Delpierre, N., Gash, J.H.C., et al. 2011. Assessing parameter variability in a photosynthesis model within and between plant functional types using global Fluxnet eddy covariance data. *Agric. For. Meteorol.* **151**(1): 22–38. doi:10.1016/j.agrformet.2010.08.013.
- Gwak, Y., and Kim, S. 2017. Factors affecting soil moisture spatial variability for a humid forest hillslope. *Hydrol. Processes*, **31**: 431–445. doi:10.1002/hyp.11039.
- Hagemann, S. 2002. An improved land surface parameter dataset for global and regional climate models. Max Planck Institute for Meteorology.
- Iio, A., Hikosaka, K., Anten, N.P.R., Nakagawa, Y., and Ito, A. 2014. Global dependence of field-observed leaf area index in woody species on climate: a systematic review: Global dependence of leaf area index on climate. *Glob. Ecol. Biogeogr.* **23**(3): 274–285. doi:10.1111/geb.12133.
- Isabelle, P.-E., Nadeau, D.F., Asselin, M.-H., Harvey, R., Musselman, K.N., Rousseau, A.N., and Anctil, F. 2018. Solar radiation transmittance of a boreal balsam fir canopy: Spatiotemporal variability and impacts on growing season hydrology. *Agric. For. Meteorol.* **263**: 1–14. doi:10.1016/j.agrformet.2018.07.022.
- Jordahl, K., den Bossche, J.V., Wasserman, J., McBride, J., Fleischmann, M., Gerard, J., Tratner, J., et al. 2019. Geopandas/geopandas: v0.6.2. doi:10.5281/zenodo.3545747.
- Kahimba, F.C., and Ranjan, R.S. 2007. Soil temperature correction of field TDR readings obtained under near freezing conditions. *Can. Biosyst. Eng.* **49**: 1.19–1.26.
- Kang, H.-S., Xue, Y., and Collatz, G.J. 2007. Impact assessment of satellite-derived leaf area index datasets using a general circulation model. *J. Clim.* **20**(6): 993–1015. doi:10.1175/JCLI4054.1.
- Kottek, M., Grieser, J., Beck, C., Rudolf, B., and Rubel, F. 2006. World map of the Köppen-Geiger climate classification updated. *Meteorol. Z.* **15**(3): 259–263. doi:10.1127/0941-2948/2006/0130.
- Kuiper, J.J., Mooij, W.M., Bragazza, L., and Robroek, B.J.M. 2014. Plant functional types define magnitude of drought response in peatland CO<sub>2</sub> exchange. *Ecology*, **95**(1): 123–131. doi:10.1890/13-0270.1.
- LaRue, E.A., Hardiman, B.S., Elliott, J.M., and Fei, S. 2019. Structural diversity as a predictor of ecosystem function. *Environ. Res. Lett.* **14**(11): 114011. doi:10.1088/1748-9326/ab49bb.
- Lasslop, G., Brovkin, V., Reick, C.H., Bathiany, S., and Kloster, S. 2016. Multiple stable states of tree cover in a global land surface model due to a fire-vegetation feedback. *Geophys. Res. Lett.* **43**: 6324–6331. doi:10.1002/2016GL069365.
- Launiainen, S., Katul, G.G., Kolari, P., Lindroth, A., Lohila, A., Aurela, M., et al. 2016. Do the energy fluxes and surface conductance of boreal coniferous forests in Europe scale with leaf area? *Global Change Biol.* **22**(12): 4096–4113. doi:10.1111/gcb.13497. PMID:27614117.
- Liu, Z., Wang, X., Chen, J.M., Wang, C., and Jin, G. 2015. On improving the accuracy of digital hemispherical photography measurements of seasonal leaf area index variation in deciduous broadleaf forests. *Can. J. For. Res.* **45**(6): 721–731. doi:10.1139/cjfr-2014-0351.
- Lu, X., Wang, Y.-P., Ziehn, T., and Dai, Y. 2013. An efficient method for global parameter sensitivity analysis and its applications to the Australian community land surface model (CABLE). *Agric. For. Meteorol.* **182–183**: 292–303. doi:10.1016/j.agrformet.2013.04.003.
- MacBean, N., Maignan, F., Peylin, P., Bacour, C., Bréon, F.-M., and Ciais, P. 2015. Using satellite data to improve leaf phenology of a global terrestrial biosphere model. *Biogeosciences*, **12**: 7185–7208. doi:10.5194/bg-12-7185-2015.
- Matheny, A.M., Mirfenderesgi, G., and Bohrer, G. 2017. Trait-based representation of hydrological functional properties of plants in weather and ecosystem models. *Plant Divers.* **39**(1): 1–12. doi:10.1016/j.pld.2016.10.001.
- McKenney, D.W., Hutchinson, M.F., Papadopol, P., Lawrence, K., Pedlar, J., Campbell, K., et al. 2011. Customized spatial climate models for North America. *Bull. Am. Meteorol. Soc.* **92**(2): 1611–1622. doi:10.1175/2011BAMS3132.1.
- Mikkelsen, K.M., Maxwell, R.M., Ferguson, I., Stednick, J.D., McGray, J.E., and Sharp, J.O. 2013. Mountain pine beetle infestation impacts: Modeling water and energy budgets at the hill-slope scale. *Ecohydrology*, **6**(1): 64–72. doi:10.1002/eco.278.
- Ministère des Forêts, de la Faune et des Parcs (MFFP). 2018. Cartographie du 5e inventaire écoforestier du Québec méridional – Méthodes et données associées, Ministère des Forêts, de la Faune et des Parcs, Secteur des forêts, Direction des inventaires forestiers. 111pp.
- Myneni, R., Knyazikhin, Y., and Park, T. 2015. MCD15A2H MODIS/Terra+Aqua Leaf Area Index/FPAR 8-day L4 Global 500m SIN Grid V006. NASA EOSDIS Land Processes DAAC. Available from <https://doi.org/10.5067/MODIS/MCD15A2H.006>.
- Oleson, K.W., and Bonan, G.B. 2000. The effects of remotely sensed plant functional type and leaf area index on simulations of boreal forest surface fluxes by the NCAR land surface model. *J. Hydrometeorol.* **1**(5): 431–446. doi:10.1175/1525-7541(2000)001<0431:TEORSP>2.0.CO;2.
- Pappas, C., Fatichi, S., and Burlando, P. 2016. Modeling terrestrial carbon and water dynamics across climatic gradients: Does plant trait diversity matter? *New Phytol.* **209**(1): 137–151. doi:10.1111/nph.13590. PMID:26389742.
- Paschalis, A., Fatichi, S., Pappas, C., and Or, D. 2018. Covariation of vegetation and climate constrains present and future T/ET variability. *Environ. Res. Lett.* **13**: 104012. doi:10.1088/1748-9326/aae267.
- Pietroniro, A., Fortin, V., Kouwen, N., Neal, C., Turcotte, R., Davison, B., et al. 2007. Development of the MESH modelling system for hydrological ensemble forecasting of the Laurentian Great Lakes at the regional scale. *Hydrol. Earth Syst. Sci.* **11**(4): 1279–1294. doi:10.5194/hess-11-1279-2007.
- Puma, M.J., Koster, R.D., and Cook, B.I. 2013. Phenological versus meteorological controls on land-atmosphere water and carbon fluxes. *J. Geophys. Res. Biogeosci.* **118**(1): 14–29. doi:10.1029/2012JG002088.
- Sterling, S., and Ducharme, A. 2008. Comprehensive data set of global land cover change for land surface model applications. *Global Biogeochem. Cycles*, **22**(3): GB3017. doi:10.1029/2007GB002959.
- Sullivan, R.C., Kotamarthi, V.R., and Feng, Y. 2019. Recovering evapotranspiration trends from biased CMIP5 simulations and sensitivity to changing climate over North America. *J. Hydrometeorol.* **20**(8): 1619–1633. doi:10.1175/JHM-D-18-0259.1.
- Ukkola, A.M., Pitman, A.J., Decker, M., De Kauwe, M.G., Abramowitz, G., Kala, J., and Wang, Y.P. 2016. Modelling evapotranspiration during precipitation deficits: Identifying critical processes in a land surface model. *Hydrol. Earth Syst. Sci.* **20**(6): 2403–2419. doi:10.5194/hess-20-2403-2016.
- van Bodegom, P.M., Douma, J.C., and Verheijen, L.M. 2014. A fully traits-based approach to modeling global vegetation distribution. *Proc. Natl. Acad. Sci. USA*. **111**(38): 13733–13738. doi:10.1073/pnas.1304551110. PMID:25225413.
- Vereecken, H., Huisman, J.A., Bogen, H., Vanderborght, J., Vrugt, J.A., and Hopmans, J.W. 2010. On the value of soil moisture measurements in vadose zone hydrology: A review. *Water Resour. Res.* **46**(4): 1–21. doi:10.1029/2008WR006829.
- Verseghy, D. 2012. CLASS – The Canadian land surface scheme (version 3.6) - technical documentation. Environment Canada Science and Technology Branch.
- Verseghy, D.L. 1991. Class – a Canadian land surface scheme for GCMS. I. Soil model. *Int. J. Climatol.* **11**: 111–133. doi:10.1002/joc.3370110202.
- Wang, L., Good, S.P., and Caylor, K.K. 2014. Global synthesis of vegetation control on evapotranspiration partitioning. *Geophys. Res. Lett.* **41**: 6753–6757. doi:10.1002/2014GL061439.
- Wei, Z., Yoshimura, K., Wang, L., Miralles, D.G., Jasechko, S., and Lee, X. 2017. Revisiting the contribution of transpiration to global terrestrial evapotranspiration. *Geophys. Res. Lett.* **44**: 2792–2801. doi:10.1002/2016GL072235.
- Wullschleger, S.D., Epstein, H.E., Box, E.O., Euskirchen, E.S., Goswami, S., Iversen, C.M., et al. 2014. Plant functional types in Earth system models: past experiences and future directions for application of dynamic vegetation models in high-latitude ecosystems. *Ann. Bot.* **114**(1): 1–16. doi:10.1093/aob/mcu077. PMID:24793697.
- Yan, K., Park, T., Yan, G., Liu, Z., Yang, B., Chen, C., et al. 2016. Evaluation of MODIS LAI/FPAR Product Collection 6. Part 2: Validation and Intercomparison. *Remote Sens.* **8**(6): 460. doi:10.3390/rs8060460.
- Zeng, Z., Zhu, Z., Lian, X., Li, L.Z., Chen, A., He, X., and Piao, S. 2016. Responses of land evapotranspiration to Earth's greening in CMIP5 Earth system models. *Environ. Res. Lett.* **11**: 104006. doi:10.1088/1748-9326/11/10/104006.
- Zeng, Z., Piao, S., Li, L.Z., Wang, T., Ciais, P., Lian, X., et al. 2018. Impact of Earth greening on the terrestrial water cycle. *J. Climate*, **31**: 2633–2650. doi:10.1175/JCLI-D-17-0236.1.
- Zhang, H., Pak, B., Wang, Y.P., Zhou, X., Zhang, Y., and Zhang, L. 2013. Evaluating surface water cycle simulated by the Australian Community Land Surface Model (CABLE) across different spatial and temporal domains. *J. Hydrometeorol.* **14**(4): 1119–1138. doi:10.1175/JHM-D-12-0123.1.
- Zhu, Z., Piao, S., Myneni, R.B., Huang, M., Zeng, Z., Canadell, J.G., et al. 2016. Greening of the Earth and its drivers. *Nat. Clim. Change*, **6**: 791–795. doi:10.1038/nclimate3004.